

# First-principles study of pressure-induced phase transition and electronic property of $\text{PbCrO}_3$

Bao-Tian Wang,<sup>1,2</sup> Wen Yin,<sup>2</sup> Wei-Dong Li,<sup>1</sup> and Fangwei Wang<sup>2,\*</sup>

<sup>1</sup>*Institute of Theoretical Physics and Department of Physics, Shanxi University, Taiyuan 030006, People's Republic of China*

<sup>2</sup>*State Key Laboratory of Magnetism, Beijing National Laboratory for Condensed Matter Physics, Institute of Physics, Chinese Academy of Sciences, Beijing 100080, People's Republic of China*

We have performed a systematic first-principles investigation to calculate the structural, electronic, and magnetic properties of  $\text{PbCrO}_3$ ,  $\text{CrPbO}_3$  as well as their equiproportional combination. The local density approximation (LDA)+ $U$  and the generalized gradient approximation+ $U$  theoretical formalisms have been used to account for the strong on-site Coulomb repulsion among the localized Cr  $3d$  electrons. By choosing the Hubbard  $U$  parameter around 4 eV within LDA+ $U$  approach, ferromagnetic, and/or antiferromagnetic ground states can be achieved and our calculated volumes, bulk moduli, and equation of states for PCO-CPO in  $R3$  phase and PCO in  $Pm\bar{3}m$  or  $R3c$  phases are in good agreement with recent experimental Phase I and Phase II [W. Xiao *et al.*, PNAS **107**, 14026 (2010)], respectively. Under pressure, phase transitions of  $R3$  PCO-CPO to  $Pm\bar{3}m$  PCO at 1.5 GPa and  $R3$  PCO-CPO to  $R3c$  PCO at -6.7 GPa have been predicted. The abnormally large volume and compressibility of Phase I is due to the content of  $\text{CrPbO}_3$  in the experimental sample and the transition of  $\text{PbO}_{6/2}$  octahedron to  $\text{CrO}_{6/2}$  upon compression. Our electronic structure study showed that there will occur an insulator-metal transition upon the phase transitions. Clear hybridization of Cr  $3d$  and O  $2p$  orbitals in wide energy range has been observed.

PACS numbers: 61.50.Ah, 71.15.Mb, 75.25.+z

## I. INTRODUCTION

Strongly correlated electron systems of transition-metal oxides with  $\text{ABO}_3$  cubic perovskite or pseudo cubic perovskite structures exhibit particular interesting physical properties. [1–4] Their ferroelectric, ferromagnetic, ferroelastic, multiferroic, and/or magnetoresistive features originate from the mutual interplay of various degrees of freedom, including lattice, spin, charge and orbital, in their partially filled B site  $3d$  electrons. The multiple chemical characters of the A ion with lone pair electrons, especially for  $\text{Bi}^{3+}$  and  $\text{Pb}^{2+}$ , also play an important role. [5, 6] Correctly describing of their electronic and magnetic structures are critical.

In late 1960s, a few groups [7–12] successfully synthesized some perovskites containing  $\text{Cr}^{4+}$  ( $\text{CaCrO}_3$ ,  $\text{SrCrO}_3$ , and  $\text{PbCrO}_3$ ) under high temperature and high pressure. For  $\text{PbCrO}_3$  (PCO), a lattice constant of about 4.00 Å for the cubic structure was determined by X-ray diffraction on single crystal and powder samples and powder neutron diffraction [7–9]. It was reported that the PCO is an antiferromagnetic (AFM) G-type semiconductor with a magnetic moment of  $\sim 1.9 \mu_B$  on each Cr ion [7, 8] and with 0.27 eV activation energy. [9] The Neel temperature ( $T_N$ ) of about 240 K was obtained by examining the magnetic and transport properties. [7, 8] For  $\text{CaCrO}_3$  and  $\text{SrCrO}_3$ , preliminary structural, magnetic, and conductive properties were also investigated. [10–

12] From then on, in a long period of more than thirty years little works had focused on these systems due to difficulty of synthesis. However, a renewed interest on them has been inspired on their transport and magnetic properties, insulator-metal transition, and pressure behaviors. [13–19] Anomalous properties of Seebeck coefficient, thermal conductivity, magnetic susceptibility, and room-temperature compressibility have been observed for  $\text{SrCrO}_3$  by Zhou *et al.* They concluded that  $\text{SrCrO}_3$  is nonmagnetic (NM) insulator and  $\text{CaCrO}_3$  is also an insulator at low temperature. But more recent studies claimed that both these perovskites are AFM metals. [18, 19] An orbital ordering transition from  $t_{2g}^2$  to  $d_{xy}^1(d_{xz}d_{yz})^1$  and electronic phase coexistence of  $C$ -AFM tetragonal and NM cubic phases have been discovered in  $\text{SrCrO}_3$ . [18] Komarek *et al.* reported that  $\text{CaCrO}_3$  is an intermediately correlated metal with similar  $C$ -type AFM ground state. Thus, whether these systems are metallic, strongly correlated, and spin ordered is still controversial. [20, 21]

Recent experimental works of PCO concentrated on its structure, electron energy loss spectroscopy, magnetic structure, and high pressure phase transition. [13–16] Electron diffraction and high-resolution electron microscopy study revealed that the microstructure of “ $\text{PbCrO}_3$ ” is a rather complex perovskite with a compositionally modulated  $a_p \times 3a_p \times (14\sim 18)a_p$  superlattice structure, where  $a_p = 4.002$  Å is the lattice constant of the cubic PCO perovskite. [13] The magnetic structure of PCO is also complex. Alario-Franco *et al.* reported AFM ordering of the chromium moments at  $T_N \sim 245$  K with a spin-reorientation at temperature range of 185 K to 62 K and their magnetic hysteresis loops for “ $\text{PbCrO}_3$ ”

\*Author to whom correspondence should be addressed; fwwang@aphy.iphy.ac.cn

suggested weak ferromagnetism at low temperature. [15] Their resistivity measurements indicated two activation energies ranges with 0.11 and 0.26 eV in different temperatures. As for pressure study, recent work performed by Xiao *et al.* [16] observed a large volume collapse in the isostructural transition of cubic PCO perovskite at  $\sim 1.6$  GPa from Phase I to Phase II. They concluded that the transition seems not related with any change of electronic state, but probably has tight relation with the abnormally large volume and compressibility of the Phase I. The real Phase I might be a kind of mixture of  $\text{PbCrO}_3$ - $\text{CrPbO}_3$  (PCO-CPO) combination due to the fact that the cubic lattice constant is enlarged if the  $\text{CrO}_{6/2}$  octahedron could be replaced by  $\text{PbO}_{6/2}$  [16].

In present study, we focus our sight on PCO, PCO-CPO, and  $\text{CrPbO}_3$  (CPO) in the cubic perovskite structure (space group  $Pm\bar{3}m$ ) and some possible distorted perovskite structures, such as  $R3c$ ,  $R3$ , and  $P4/mmm$  phases. Electronic and magnetic properties as well as pressure behaviors have been systematically investigated by the first-principles electronic structure calculations based on density functional theory (DFT) and DFT+ $U$  schemes due to Dudarev *et al.* [22] The validity of the ground-state calculation is carefully tested. Our calculated lattice parameter and bulk modulus  $B$  for cubic PCO are well consistent with previous local density approximation (LDA) and generalized gradient approximation (GGA) results [16]. The total energy, lattice constant, bulk modulus  $B$ , and spin moment of Cr ion for NM, ferromagnetic (FM), and AFM phases calculated in wide range of effective Hubbard  $U$  parameter are presented and our calculated results within LDA+ $U$  with  $U=3-4$  eV for PCO in  $Pm\bar{3}m$  or  $R3c$  phases and PCO-CPO in  $R3$  phase accord well with experimental [16] Phase II and Phase I, respectively. Our calculated spin moment by LDA+ $U$  is in good agreement with recent experimental value of saturation moment  $M_{\text{sat}}=1.70 \mu_B$ , which is deduced from the effective moment  $M_{\text{eff}}=2.51 \mu_B$  [15] according to the relation  $M_{\text{eff}}=2[S(S+1)]^{1/2}=[M_{\text{sat}}(M_{\text{sat}}+2)]^{1/2}$ . The P-V relations of PCO and PCO-CPO are calculated to compare with experiment. The insulting property of “ $\text{PbCrO}_3$ ” at ambient condition is successfully predicted.

## II. COMPUTATIONAL METHODS

First-principles DFT calculations on the basis of the frozen-core projected augmented wave (PAW) method of Blöchl [23] are performed within the Vienna *ab initio* simulation package (VASP) [24], where the exchange and correlation effects are described by the DFT within LDA and GGA [25, 26]. For the plane-wave set, a cutoff energy of 500 eV is used. The  $k$ -point meshes in the full wedge of the Brillouin zone (BZ) are sampled by  $12 \times 12 \times 12$  and  $6 \times 6 \times 6$  grids according to the Monkhorst-Pack [27] scheme for PCO, CPO, and PCO-CPO in their cubic and rhombohedral unit cells, respectively. The cu-

bic perovskite structure are built for nonmagnetic (NM) and ferromagnetic (FM) calculations and the rhombohedral unit cells (Fig. 1) for G-type antiferromagnetic (AFM) configuration, which is  $(\frac{1}{2}, \frac{1}{2}, \frac{1}{2})$  order in terms of the original perovskite cell. The rhombohedral unit cell for PCO in its cubic structure is constructed using the  $R3c$  space group ( $\alpha=60^\circ$ ) with Pb atoms in  $2a(0, 0, 0)$  site, Cr in  $2a(\frac{1}{4}, \frac{1}{4}, \frac{1}{4})$  site, and O in  $6b(\frac{1}{2}, 0, \frac{1}{2})$  site. Moving away slightly atoms from these high symmetry positions will lower the symmetry and consequently build the cell in real  $R3c$  or  $R3$  phase. In this study, the Pb  $5d^{10}6s^26p^2$ , Cr  $3d^54s^1$ , and O  $2s^22p^4$  orbitals are explicitly included as valence electrons. The strong on-site Coulomb repulsion among the localized Cr  $3d$  electrons is described by using the formalism formulated by Dudarev *et al.* [22]. In this scheme, the total LDA (GGA) energy functional is of the form

$$E_{\text{LDA(GGA)+U}} = E_{\text{LDA(GGA)}} + \frac{U-J}{2} \sum_{\sigma} [\text{Tr} \rho^{\sigma} - \text{Tr}(\rho^{\sigma} \rho^{\sigma})], \quad (1)$$

where  $\rho^{\sigma}$  is the density matrix of  $d$  states with spin  $\sigma$ , while  $U$  and  $J$  are the spherically averaged screened Coulomb energy and the exchange energy, respectively. In this work, the Coulomb  $U$  is treated as one variable, while the parameter  $J$  is set to 0.5 eV. Since only the difference between  $U$  and  $J$  is meaningful in Dudarev's approach, therefore, we label them as one single parameter  $U$  for simplicity. To obtain the energy data under different pressures, we perform the structure-relaxation calculations at a series of fixed volumes. The corresponding pressure values are deduced from the energy-volume data by  $P=-\partial E/\partial V$ .

## III. RESULTS

### A. Structural and magnetic properties of cubic PCO

Both spin-unpolarized and spin-polarized calculations are performed for cubic PCO. For NM, FM, and AFM configurations, the total energies (-39.685 eV, -39.706 eV, and -39.818 eV, respectively) calculated within the DFT ( $U=0$ ) have no visible differences. After turning on the Hubbard  $U$ , the NM phase is not energetically favorable both in the LDA+ $U$  and GGA+ $U$  formalisms compared with FM and AFM phases. In the following, we only present results of FM and AFM configurations. The dependences of total-energy differences (per formula unit at respective optimum geometries) between FM and AFM ( $E_{\text{FM}}-E_{\text{AFM}}$ ), lattice parameter, bulk modulus, and spin moments of Cr ions on  $U$  for cubic PCO are shown in Fig. 2. The theoretical equilibrium volume, bulk modulus  $B$ , and pressure derivative of the bulk modulus  $B'$  are obtained by fitting the third-order Birch-Murnaghan equation of state (EOS) [28]. For com-

parison, recent experimental values [16] of  $a_0$  and  $B$  for Phase I and Phase II as well as the experimental results of spin magnetic moment of Cr ions are also shown. In LDA or GGA ( $U=0$  eV), the total energy of AFM phase is lower than that of FM phase. However, as shown in Fig. 2(a), the total energy of the FM phase decreases to become lower than that of the AFM phase when increasing  $U$ . At a typical value of  $U=4$  eV, the total-energy differences between FM and AFM ( $E_{\text{FM}}-E_{\text{AFM}}$ ) reach their minimums of  $-74$  meV and  $-91$  meV within the LDA+ $U$  and GGA+ $U$  formalisms, respectively. Note that we have also considered other types of AFM configurations and our results show that the  $G$ -AFM in  $(\frac{1}{2}, \frac{1}{2}, \frac{1}{2})$  order is the most stable state. These results are consistent with recent experimental observations [15], where they reported the AFM ordering of the chromium moments at  $T_N \sim 245$  K with a spin-reorientation at temperature range of 185 K to 62 K and their magnetic hysteresis loops for “PbCrO<sub>3</sub>” suggested weak ferromagnetism at low temperature. As clearly shown in Fig. 2(b), our calculated lattice parameters of cubic PCO within two DFT+ $U$  approaches are all by large smaller than the experimental value  $a_0=4.013$  Å [7–9, 16] of Phase I. Corresponding results of bulk modulus are dramatically bigger than that obtained by experiment ( $B=59$  GPa) for Phase I [Fig. 2(c)]. But the experimental lattice parameter  $a_0=3.862$  Å and bulk modulus  $B=187$  GPa of Phase II well lies in the range of our calculated results of cubic PCO, which supports their conclusion of cubic PCO perovskite [16] that the real Phase I might be a kind of mixture of random PCO-CPO combination. In next subsection, we will discuss carefully the structural properties of PCO-CPO.

As shown in Fig. 2, the tendencies of  $a_0$ ,  $B$ , and spin moments of Cr ions for FM phase with  $U$  are similar to that of the AFM phase. Results of NM phase (not presented) further indicates its unstable nature at low temperature. As shown in Fig. 2(b), LDA underestimates the lattice parameter with respect to the experimental value while GGA coincides well with experiment. Our LDA and GGA results for NM phase accords well with previous first-principle calculations [16]. Result of LDA is due to its typical overbinding character. The LDA+ $U$  method will lead to relative larger equilibrium volume compared to the LDA and therefore improves the agreement with experiment, especially for FM and AFM phases. At a typical value  $U=4$  eV, the LDA+ $U$  gives  $a_0=3.822$  Å for AFM cubic PCO which is very close to the experimental value. On the other hand, the GGA+ $U$  enlarges the underbinding effect with increasing Hubbard  $U$ . As a comparison, at  $U=4$  eV, the GGA+ $U$  gives  $a_0=3.921$  Å. As for the dependence of bulk modulus  $B$  on  $U$  shown in Fig. 2(c), it is clear that the LDA results (230-153 GPa) are always higher than the GGA results (187-113 GPa), which is due to the above mentioned underbinding effect of the GGA approach. At a typical value  $U=4$  eV, the LDA+ $U$  and GGA+ $U$  give  $B=198$  ( $B'=4.6$ ) and 148 GPa ( $B'=5.1$ ) for AFM cubic

PCO, respectively. Obviously, result calculated within LDA+ $U$  with  $U=4$  eV is consistent with the experimental value of  $B=187$  GPa [16]. For the dependence of spin moments of Cr ions on  $U$  shown in Fig. 2(d), we see clear increasing amplitude of magnetic moments with  $U$  for both FM and AFM phases. Our calculated value of  $1.47 \mu_B$  using LDA for AFM phase is in good agreement with previous LMTO calculation value of  $1.414 \mu_B$  [29]. At a typical value  $U=4$  eV, the LDA+ $U$  and GGA+ $U$  give magnetic moments of  $2.46$  and  $2.62 \mu_B$  for AFM PCO, respectively, both of which exceed recent experimental value of  $1.70 \mu_B$  [15]. Similar trend has also been exhibited in study of BiFeO<sub>3</sub> [5]. Therefore, inclusion of on-site Coulomb energy for adequately describing the structural and magnetic properties is crucial. In study of CrO<sub>2</sub>, x-ray absorption and resonant photoemission spectroscopy support the importance of Coulomb correlations [30]. Huang *et al.* concluded that the on-site Coulomb interaction energy of CrO<sub>2</sub> is 3-4 eV through comparing their experimental measurements and LDA+ $U$  calculations. They found that the shift of Cr  $3d$  spin-up DOS slightly away from the Fermi level increases the Cr spin moment. In our present study, similar shift of Cr  $3d$  DOS is also observed (see below). Overall, comparing with the experimental data, the accuracy of our atomic-structure prediction for AFM cubic PCO is quite satisfactory by tuning the effective Hubbard parameter  $U$  in a range of 3-4 eV within the LDA+ $U$  approach, which supplies the safeguard for our following study of electronic structure and pressure behaviors of PCO. In following study, we present our results within LDA and LDA+ $U$  with constant  $U=4$  eV.

## B. Phase transition analysis

After previous analysis, one question arises: What’s the ground state of experimentally observed “PbCrO<sub>3</sub>” at ambient condition. In this section, we will test carefully the ground state of “PbCrO<sub>3</sub>” by calculating the total energies of PCO, PCO-CPO, and CPO in cubic perovskite structure and some possible distorted perovskite structures. Their relative energies in  $G$ -AFM configuration calculated within LDA+ $U$  are shown in Fig. 3. Clearly, although the equilibrium lattice parameter (3.998 Å) for  $Pm\bar{3}m$  phase of PCO-CPO accords well with experimental data of Phase I [16], the  $Pm\bar{3}m$  phase of PCO-CPO and CPO are not energetically favorable in the whole range of volume. After testing various possible crystal structures and atomic arrangements, we find that  $R3c$  phase of PCO and  $R3$  phase of PCO-CPO possess same energy level with that of cubic PCO in some volumes. In the whole range of volume,  $R3c$  PCO is more energetically favorable than cubic PCO. Considering this material only can be synthesized under high temperature and high pressure, the high-pressure phase of PCO can be understood as crystallizing in  $Pm\bar{3}m$  or  $R3c$  structure. Increasing the cell volume, as shown in Fig. 3,

the  $R3$  PCO-CPO becomes more energetically favorable than the two high-pressure phases. This clearly indicates that the structure of “PbCrO<sub>3</sub>” at ambient pressure is  $R3$  PCO-CPO. Therefore, upon compression there will occur structural phase transition among the three phases. As shown in the inset of Fig. 3, phase transitions of  $R3$  PCO-CPO to  $Pm\bar{3}m$  PCO at 1.5 GPa and  $R3$  PCO-CPO to  $R3c$  PCO at -6.7 GPa can be predicted by the slopes of the common tangent rule. The former value coincides well with recent experimentally observed value of 1.6 GPa, while the latter value is smaller than that. As a result, the crystal structures of PCO under high pressure need more works to clarify. Our present study give two most possible structures:  $Pm\bar{3}m$  or  $R3c$ . Concerning the energetics of the transitions from  $R3$  PCO-CPO to  $Pm\bar{3}m$  PCO at 1.5 GPa and from  $R3$  PCO-CPO to  $R3c$  PCO at -6.7 GPa, Fig. 3 clearly shows that per formula unit of PCO-CPO needs 97 meV and 458 meV of energy, respectively.

In Table I, we present the calculated lattice parameters for PCO in  $R3c$  phase and PCO-CPO in  $R3$  structure. It can be found that the equilibrium volume of  $R3c$  PCO is consistent with that of experimental Phase II and  $R3$  PCO-CPO comparable to Phase I [16]. Although Xiao *et al.* reported that both the Phase I and Phase II crystallize in cubic perovskite structure, our calculations are different from their observations. Our present results need more experimental works to test. For  $R3c$  PCO and  $R3$  PCO-CPO, our calculated values of  $E_{\text{FM}}-E_{\text{AFM}}$  (per formula unit) are -80 meV and -62 meV within the LDA+ $U$  formalism, respectively, the corresponding bulk moduli  $B=164$  ( $B'=7.9$ ) and 153 GPa ( $B'=4.3$ ) for AFM phase, respectively,  $B=157$  ( $B'=5.6$ ) and 150 GPa ( $B'=4.4$ ) for FM phase, respectively, and spin moments of Cr ions are 2.79 and 2.92  $\mu_B$  for AFM configuration, respectively. Averaged to every Cr<sup>4+</sup> ion, the  $E_{\text{FM}}-E_{\text{AFM}}$  of  $R3$  PCO-CPO is about -31 meV, which is almost consistent with recent experimental report [15] of the AFM ordering at  $T_N \sim 245$  K. For the bulk moduli, values of  $R3c$  PCO are slightly smaller than the experimental value of Phase II  $B=187$  GPa [16], while values of  $R3$  PCO-CPO are prominently larger than the experimental value of Phase I. The abnormal high compressibility of Phase I is due to the fact that the CrO<sub>6/2</sub> to PbO<sub>6/2</sub> transition has been compressed to occur under low pressure (see below). For spin moments, results of FM phase are almost equal to the AFM phase for PCO-CPO in  $R3$  phase and PCO in both  $Pm\bar{3}m$  and  $R3c$  phases.

### C. Pressure behaviors

The equation of states of AFM PCO-CPO in  $Pm\bar{3}m$  and  $R3$  phases, AFM PCO in  $Pm\bar{3}m$  and  $R3c$  phases, and the experimental measured pressure-volume data from Ref. [[16]] are presented in Fig. 4. For  $Pm\bar{3}m$  and  $R3c$  phases of PCO ( $R3$  phase of PCO-CPO), the relative smaller volumes calculated in our scheme compared with

TABLE I: Calculated lattice constant  $a$ , rhombohedral angle  $\alpha$ , volume  $V$ , and Wyckoff parameters for PCO in  $R3c$  phase and PCO-CPO in  $R3$  structure. For  $R3c$  phase, the Wyckoff positions  $2a$  ( $x, x, x$ ) and  $6b$  ( $x, y, z$ ) refer to the cations and anions, respectively. In case of the  $R3$  structure, the corresponding Wyckoff labels are  $1a$  ( $x, x, x$ ) and  $3b$  ( $x, y, z$ ).

		PCO	PCO-CPO
space group		$R3c$	$R3$
$a$ [Å]		5.381	5.800
$\alpha$ [°]		60.86	55.12
$V$ [Å <sup>3</sup> ]		112.33	122.31
Pb	$x$	0.977	0.987/0.729
Cr	$x$	0.218	0.209/0.525
O	$x$	0.542	0.533/0.436
	$y$	0.958	0.924/0.139
	$z$	0.392	0.377/0.815

experimental Phase II (Phase I) originates from the typical overbinding character of LDA. From Fig. 4, one can find that our calculated volume collapses of  $Pm\bar{3}m$  PCO-CPO to  $Pm\bar{3}m$  PCO and  $R3$  PCO-CPO to  $R3c$  PCO at experimental phase transition pressure 1.6 GPa is about 12.4% and 8.0%, respectively. The former value is larger than the measured value (9.8%) in recent experiments [16], while the latter value is smaller than that. Underestimation of the volume collapse value, from  $R3$  PCO-CPO to  $R3c$  PCO, can be attributed to the experimental fact that the CrO<sub>6/2</sub> to PbO<sub>6/2</sub> transition has been compressed to occur under low pressure of around 0.1-1.6 GPa in the experimental compound “Phase I”. This kind of partial transition leads to abnormal high compressibility of Phase I compared with CaCrO<sub>3</sub>, SrCrO<sub>3</sub>, and high-pressure Phase II of PbCrO<sub>3</sub> [16, 17].

### D. Electronic structure

Figure 5 shows the total density of states (DOS) as well as the projected DOS for the Cr 3*d*, Cr 4*s*, and O 2*p* orbitals for AFM PCO in  $Pm\bar{3}m$  and  $R3c$  phases and AFM PCO-CPO in  $R3$  phase at selective values of  $U$  within LDA+ $U$  formalism. Corresponding band-structures calculated with  $U=4$  eV are presented in Fig. 6, where both spin-up and spin-down results are plotted. Since spin-down results for PCO in  $Pm\bar{3}m$  and  $R3c$  phases are same with their spin-up results, as indicated in Figs. 6(a)-6(b), we only plot in Figs. 5(a)-5(d) the spin-up results. For AFM PCO-CPO in  $R3$  phase, slight differences between spin-up and spin-down can be seen in Figs. 5(e) and 6(c). Overall, results of PCO in both  $Pm\bar{3}m$  and  $R3c$  phases indicate that the AFM PCO is metallic without accounting for or after switching on the on-site Coulomb repulsion [see Figs. 5(a)-5(d) and 6(a)-6(b)]. This fact conflicts with the experimental observations that the “PbCrO<sub>3</sub>” is AFM semiconductor with

0.27 eV or 0.11 eV activation energy in different temperature ranges [9, 15]. In our calculations even increasing the amplitude of  $U$  up to 8 eV, the metallic state has not changed for these two phases of PCO. The metallic ground states have also been observed for NM and FM phases. Besides, inclusion of the spin-orbit coupling (SOC) and noncollinearity also can not open a gap at the Fermi level. Thus, we only can conclude that the high-pressure phase of  $\text{PbCrO}_3$  is a conductor. Additionally, results of CPO and PCO-CPO in  $Pm\bar{3}m$  phase also show that they are conductors. Although a gap is opened with the Hubbard  $U=6$  eV for  $Pm\bar{3}m$  PCO-CPO (not shown), the calculated insulating band gap (2.12 eV) is prominently larger than the experimental values [9, 15]. In present study, we prefer to believe that the LDA+ $U$  with  $U=4$  eV can give a correct depictions of the ground state electronic structures for PCO and PCO-CPO. For AFM PCO-CPO in  $R3$  phase, our LDA+ $U$  with  $U=4$  eV calculation open an insulating band gap of about 0.48 eV [see Fig. 5(e) and 6(c)]. Figure 6(c) clearly indicates that the valence band maximum (VBM) appear at Z point and conduction band minimum (CBM) at  $\Gamma$  point in BZ. We find that both VBM and CBM have predominant O  $2p$  state character mixed with significant Cr  $3d$  contribution. Although the calculated value of band gap (0.48 eV) is almost two times of the experimental value 0.27 eV [9, 15], since the activation energy of the Phase I perovskite increases with lowing temperature [15], we believe that our calculation (valid only at 0 K) can give a proper depictions of the electronic structures for low-pressure phase of  $\text{PbCrO}_3$ . Our calculations clearly illustrate that the “ $\text{PbCrO}_3$ ” will occur an insulator-metal transition together with the phase transition of  $R3$  PCO-CPO to  $Pm\bar{3}m/R3c$  PCO upon compression.

We note that the conductivity of  $\text{SrCrO}_3$  and  $\text{CaCrO}_3$  exists controversial [17–21]. Theoretical calculation for  $\text{CaCrO}_3$  [20] predicted metallic ground state with LDA and insulating state with LDA+ $U$ . For  $\text{SrCrO}_3$  [21], the metallic ground state was observed either with LDA or LDA+ $U$ . Besides, using LDA+ $U$  method with  $U=4$  eV, Lee *et al.* [21] successfully predicted an orbital-ordering transition from  $t_{2g}^2$  to  $d_{xy}^1(d_{xz}d_{yz})^1$  for  $\text{SrCrO}_3$ . No evidence of orbital ordering within the  $t_{2g}$  shell for  $\text{CaCrO}_3$  was observed [19]. In our study of PCO, CPO, and PCO-CPO compounds, this kind of orbital ordering in Cr  $t_{2g}$  states has also not been found.

As shown in Fig. 5, inclusion of the on-site Coulomb repulsion will lower the occupation energy of Cr  $3d$  electrons from the Fermi level and elevate Cr  $4s$ , Cr  $4s$ , and O  $2p$  orbitals occupation levels near  $-7.0$  eV to high level. As a result, localization pictures of electrons occupation appear after introducing the Coulomb repulsion. From Figs. 5(c)-5(e), one can find that the Cr  $4s$  contribution is limited. When Cr ions combining with O ions to form covalent/ionic bonds, part of Cr  $3d$  and Cr  $4s$  electrons will transfer to O  $2p$  orbital. This kind of electron transfer behavior can be read from the partial DOS pictures. Considering the effect of  $d$ -hole creation due to  $3d$ - $4s$  hybridization, we have also examined the effect of Coulomb

repulsion on Cr  $4s$ -shell. However, no difference of Cr  $4s$  orbital has been found for introducing the Coulomb repulsion into the  $d$ -shell or the  $s$ -shell. In Figs. 5 and 6, only  $d$ -shell is considered to participate in the Coulomb exchange. In the whole energy domain, electronic structures of AFM PCO in  $Pm\bar{3}m$  and  $R3c$  phases have no evident differences. The main occupation at the Fermi level is from Cr  $3d$  and O  $2p$  orbitals. Our results calculated at  $U=0$  eV are consistent with previous calculations [29]. A clear hybridization of Cr  $3d$  and O  $2p$  orbitals in the energy range from  $-7.3$  to  $0.3$  eV can be observed at  $U=0$  eV. After switching on the  $U$  to 4 eV, this hybridization energy range is moved to from  $-6.2$  to  $0.2$  eV. A well resolved peak of Cr  $3d$  state at around  $-0.3$  eV at  $U=0$  eV is flatted when the Hubbard  $U$  parameter being increased to about 4 eV. In addition, a band gap in the conduction band is apparent under  $U=0$  to 6 eV. This band gap increases from 0.6 eV at  $U=0$  eV to about 2.0 eV at  $U=4$  eV. The main occupation in the conduction band is from Cr  $3d$  orbital with some contribution from O  $2p$  states. For AFM PCO-CPO in  $R3$  phase, hybridization of Cr  $3d$  and O  $2p$  orbitals in the energy range from  $-6.3$  to  $-1.0$  eV is clear. One narrow peak locates just below the Fermi level.

#### IV. CONCLUSIONS

In conclusion, the ground state properties as well as the high pressure behaviors of PCO, CPO, and PCO-CPO compounds were studied by means of the first-principles DFT+ $U$  method. By choosing the Hubbard  $U$  parameter around 4 eV within the LDA+ $U$  approach, FM and/or AFM ground states were achieved and our calculated volumes, bulk moduli, spin moments, and equation of states are in good agreement with recent experiments. While the PCO-CPO in  $R3$  phase is consistent with the experimental low-pressure Phase I, both  $Pm\bar{3}m$  and  $R3c$  phases of PCO coincide well with high-pressure Phase II. Specially, the semiconductor nature of  $R3$  PCO-CPO is in good agreement with experiments. These observations explicitly indicate the existence of strongly correlated electronic behaviors in these compounds. Our electronic spectrums illustrate a clear hybridization of Cr  $3d$  and O  $2p$  orbitals in wide energy range. In contrast to  $\text{SrCrO}_3$ , the orbital-ordering transition from  $t_{2g}^2$  to  $d_{xy}^1(d_{xz}d_{yz})^1$  has not been found in these materials.

#### Acknowledgments

We are grateful to O. Eriksson for useful discussions. This work was supported by the National Basic Research Program of China (973 Program) (Grant No. 2010CB833102) and the National Natural Science Foundation of China (Grant Nos. 11104170, 10974244, and 11074155).

- 
- [1] W. Zhong and D. Vanderbilt, Phys. Rev. Lett. **74**, 2587 (1995).
- [2] M. Imada, A. Fujimori, Y. Tokura, Rev. Mod. Phys. **70**, 1039 (1998).
- [3] Y. Tokura, and N. Nagaosa, Science, **288**, 462 (2000).
- [4] E. Dagotto, Science, **309**, 257 (2005).
- [5] J. B. Neaton, C. Ederer, U. V. Waghmare, N. A. Spaldin, and K. M. Rabe, Phys. Rev. B **71**, 014113 (2005).
- [6] S. Picozzi and C. Ederer, J. Phys.: Condens. Matter **21**, 303201 (2009).
- [7] W. L. Roth and R. C. DeVries, J. Appl. Phys. **38**, 951 (1967).
- [8] R. C. DeVries and W. L. Roth, J. Am. Ceram. Soc. **51**, 72 (1968).
- [9] B. L. Chamberland and C. W. Moeller, J. Solid State Chem. **5**, 39 (1972).
- [10] B. L. Chamberland, Solid State Commun. **5**, 663 (1967).
- [11] J. B. Goodenough, J. M. Longo, and J. A. Kafalas, Mater. Res. Bull. **3**, 471 (1968).
- [12] J. F. Weiher, B. L. Chamberland, and J. L. Gillson, J. Solid State Chem. **3**, 529 (1971).
- [13] Á. M. Arévalo-López and M. Á. Alario-Franco, J. Solid State Chem. **180**, 3271 (2007).
- [14] Á. M. Arévalo-López, E. Castillo-Martínez, and M. Á. Alario-Franco, J. Phys.: Condens. Matter **20**, 505207 (2008).
- [15] Á. M. Arévalo-López, A. J. D. Santos-García, and M. Á. Alario-Franco, Inorg. Chem. **48**, 5434 (2009).
- [16] W. Xiao, D. Tan, X. Xiong, J. Liu, and J. Xu, PNAS **107**, 14026 (2010).
- [17] J.-S. Zhou, C.-Q. Jin, Y.-W. Long, L.-X. Yang, and J. B. Goodenough, Phys. Rev. Lett. **96**, 046408 (2006).
- [18] L. O. SanMartin, A. J. Williams, J. Rodgers, J. P. Attfield, G. Heymann, and H. Huppertz, Phys. Rev. Lett. **99**, 255701 (2007).
- [19] A. C. Komarek, S. V. Streltsov, M. Isobe, T. Moller, M. Hoelzel, A. Senyshyn, D. Trots, M. T. Fernández-Díaz, T. Hansen, H. Gotou, T. Yagi, Y. Ueda, V. I. Anisimov, M. Gruninger, D. I. Khomskii, and M. Braden, Phys. Rev. Lett. **101**, 167204 (2008).
- [20] S. V. Streltsov, M. A. Korotin, V. I. Anisimov, and D. I. Khomskii, Phys. Rev. B **78**, 054425 (2008).
- [21] K. W. Lee and W. E. Pickett, Phys. Rev. B **80**, 125133 (2009).
- [22] S. L. Dudarev, G. A. Botton, S. Y. Savrasov, C. J. Humphreys, and A. P. Sutton, Phys. Rev. B **57**, 1505 (1998).
- [23] P. E. Blöchl, Phys. Rev. B **50**, 17953 (1994).
- [24] G. Kresse and J. Furthmüller, Phys. Rev. B **54**, 11169 (1996).
- [25] W. Kohn and L. J. Sham, Phys. Rev. **140**, A1133 (1965).
- [26] J. P. Perdew, K. Burke, and Y. Wang, Phys. Rev. B **54**, 16533 (1996).
- [27] H. J. Monkhorst and J. D. Pack, Phys. Rev. B **13**, 5188 (1972).
- [28] F. Birch, Phys. Rev. **71**, 809 (1947).
- [29] S. Mathi Jaya, R. Jagadish, R. S. Rao, and R. Asokamani, Mod. Phys. Lett. B **6**, 103 (1992).
- [30] Yu. S. Dedkov, A. S. Vinogradov, M. Fonin, C. König, D. V. Vyalikh, A. B. Preobrajenski, S. A. Krasnikov, E. Yu. Kleimenov, M. A. Nesterov, U. Rüdiger, S. L. Molodtsov, and G. Güntherodt, Phys. Rev. B **72**, 060401(R) (2005); D. J. Huang, H.-T. Jeng, C. F. Chang, G. Y. Guo, J. Chen, W. P. Wu, S. C. Chung, S. G. Shyu, C. C. Wu, H.-J. Lin, and C. T. Chen, *ibid.* **66**, 174440 (2002); M. A. Korotin, V. I. Anisimov, D. I. Khomskii, and G. A. Sawatzky, Phys. Rev. Lett. **80**, 4305 (1998); T. Tsujioka, T. Mizokawa, J. Okamoto, A. Fujimori, M. Nohara, H. Takagi, K. Yamaura, and M. Takano, Phys. Rev. B **56**, R15509 (1997).

Figure captions:

Fig. 1: (Color online) Pictorial illustrations of (a) cubic PCO and (b) cubic PCO-CPO in AFM configuration. For PCO-CPO, the first atom along the [111] diagonal direction is labeled as Pb1, second Cr1, third Cr2, and fourth Pb2. One can find that along [111] direction in PCO the Pb and Cr alternate while in PCO-CPO the Pb and Cr alternate in pairs. Compared with PCO, in PCO-CPO half percent of the A site and B site atoms are exchanged while in CPO the A site and B site atoms are totally exchanged.

Fig. 2: (Color online) Dependences of (a) total-energy differences (per formula unit) between FM and AFM ( $E_{\text{FM}} - E_{\text{AFM}}$ ), (b) lattice parameter, (c) bulk modulus, and (d) spin moments of Cr ions on  $U$  for AFM PCO in  $Pm\bar{3}m$  structure.

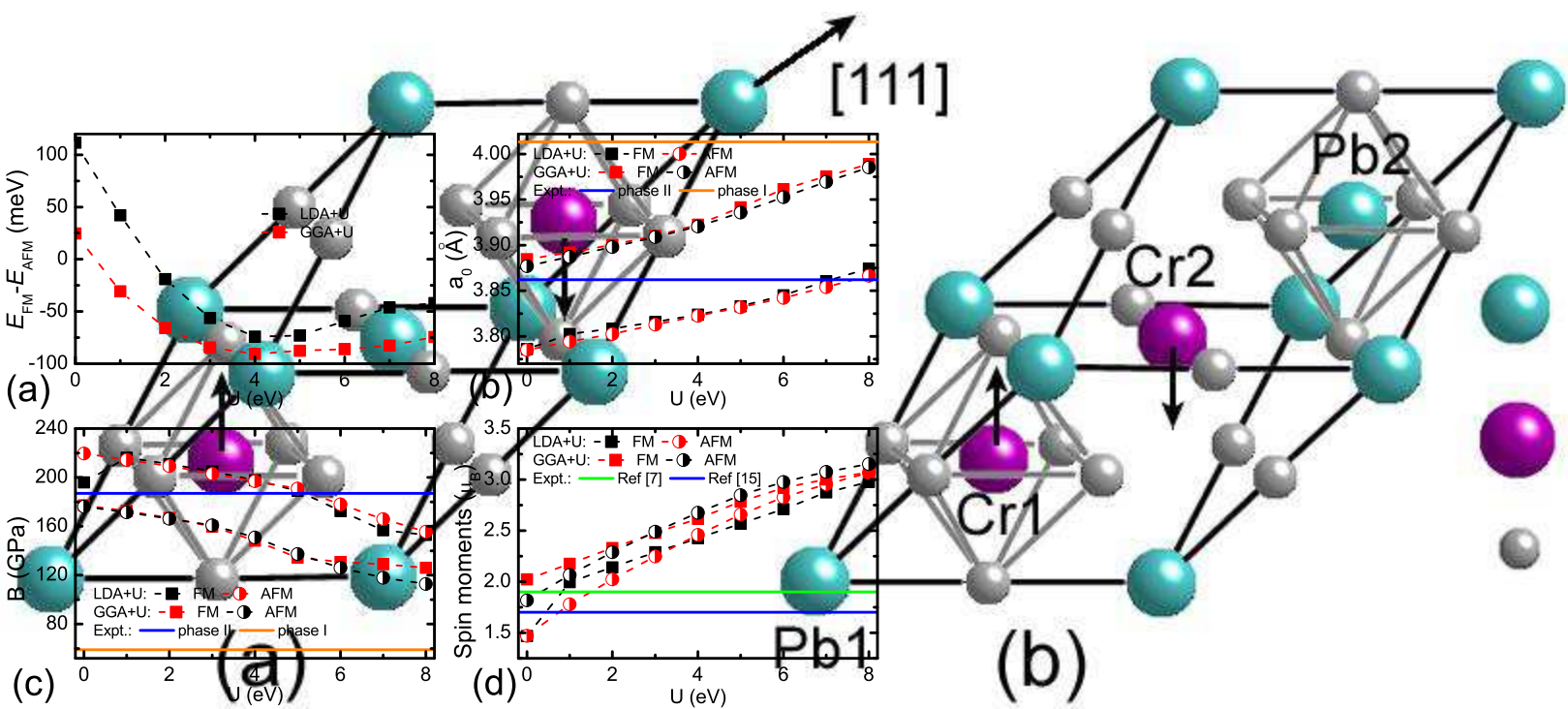
Fig. 3: (Color online) Comparison of relative energies of two unit cells of AFM PCO in  $Pm\bar{3}m$  and  $R3c$  phases, one formula unit of AFM PCO-CPO in  $Pm\bar{3}m$  and  $R3$  phases, and two unit cells of AFM CPO in  $Pm\bar{3}m$  phase vs the volume. All results are calculated within LDA+ $U$  at  $U=4$  eV. Phase transitions of  $R3$  PCO-CPO to  $Pm\bar{3}m$

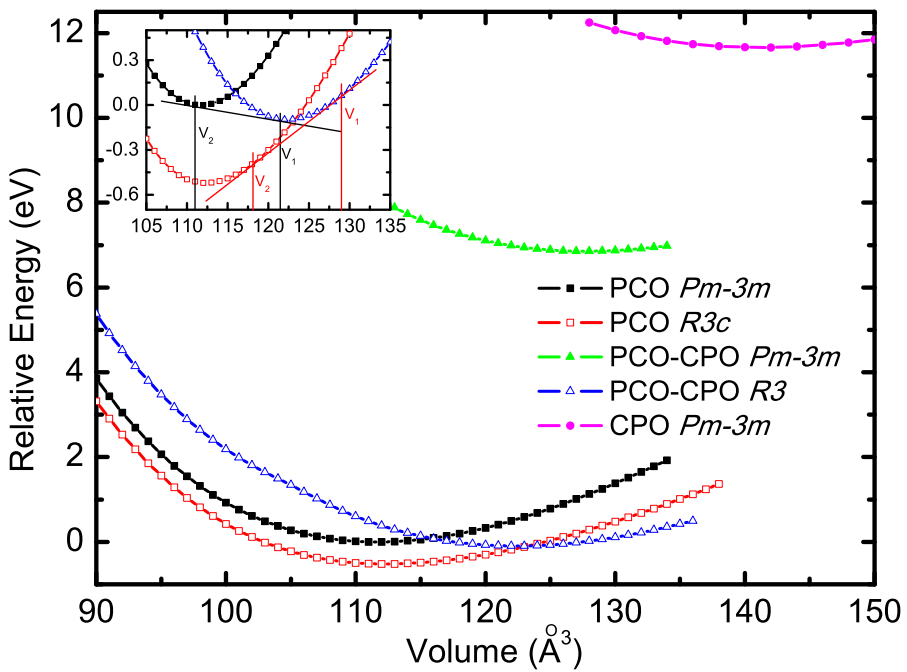
PCO at 1.5 GPa and  $R3$  PCO-CPO to  $R3c$  PCO at -6.7 GPa can be predicted by the slopes of the common tangent rule, as shown in the inset.

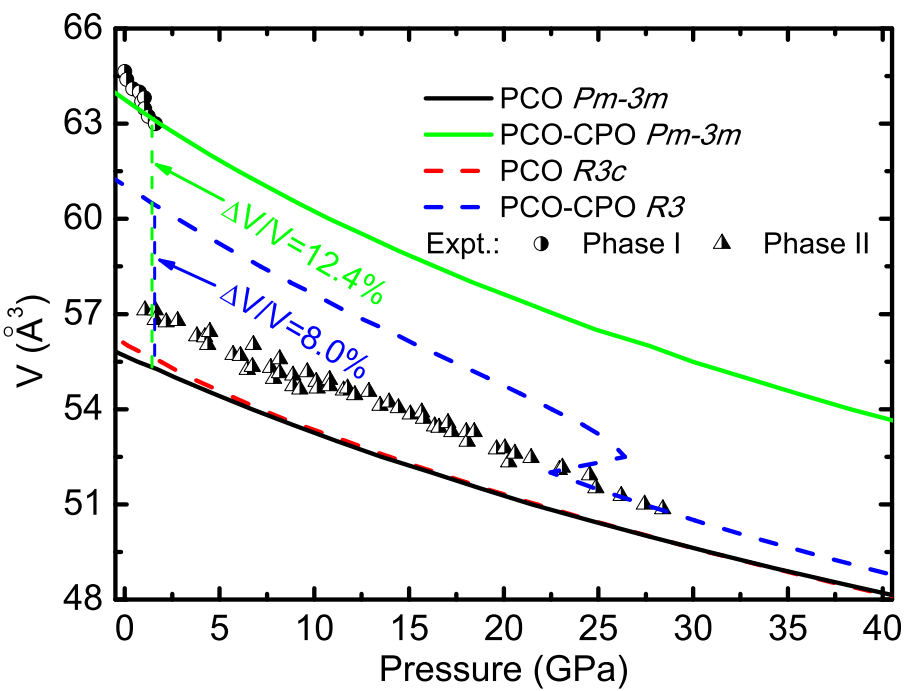
Fig. 4: (Color online) The P-V relations of the AFM PCO-CPO in  $Pm\bar{3}m$  and  $R3$  phases as well as AFM PCO in  $Pm\bar{3}m$  and  $R3c$  phases computed in the LDA+ $U$  formalism. Experimental results from Ref. [16] are also presented. The volume collapses at experimental phase transition pressure 1.6 GPa are labeled.

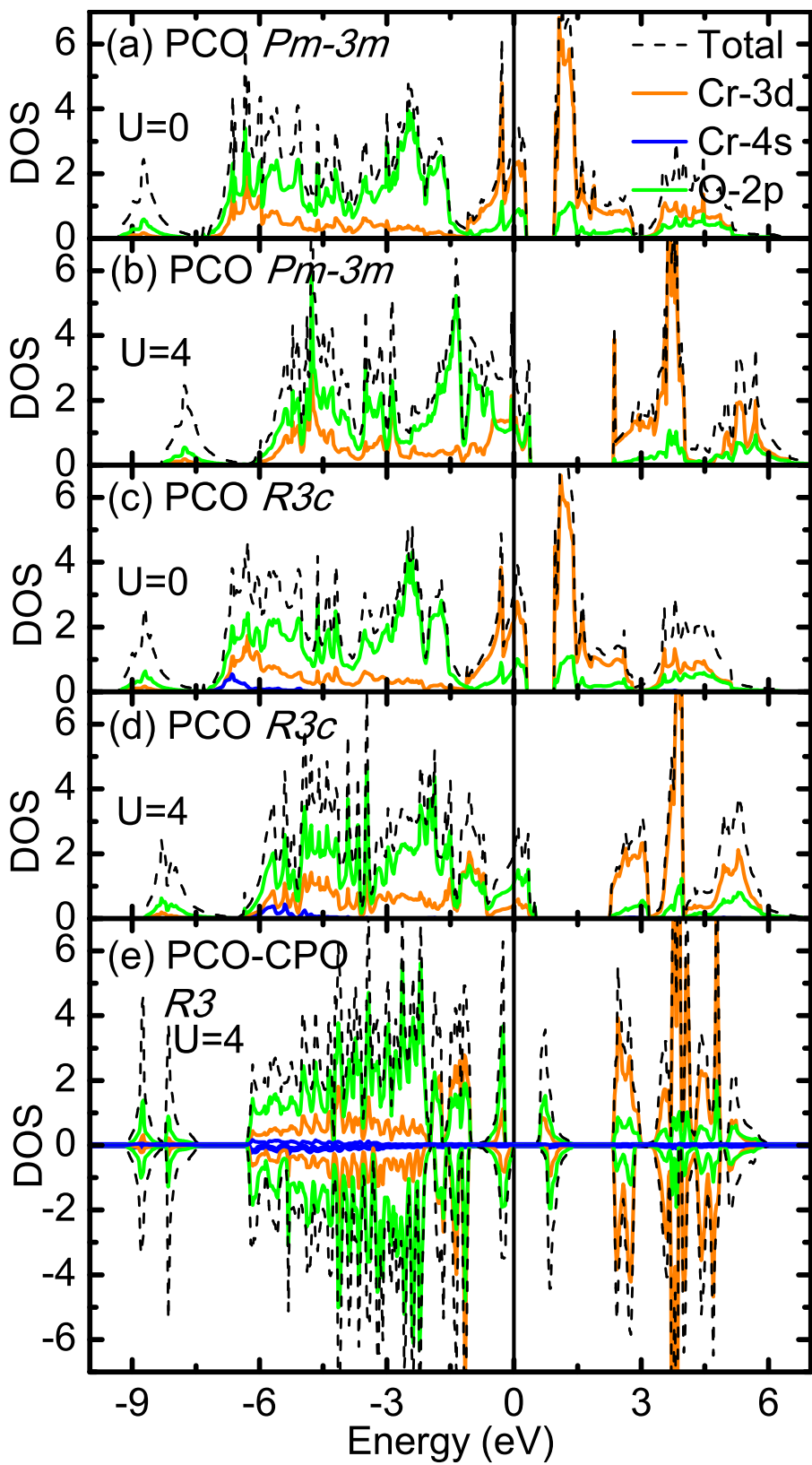
Fig. 5: (Color online) The total DOS for AFM PCO in  $Pm\bar{3}m$  and  $R3c$  phases as well as AFM PCO-CPO in  $R3$  phase computed in the LDA+ $U$  formalism with selective values of  $U$ . The projected DOSs for the Cr  $3d$ , Cr  $4s$ , and O  $2p$  orbitals are also shown. In panel (e), both spin-up and spin-down results are presented. The Fermi energy level is set at zero.

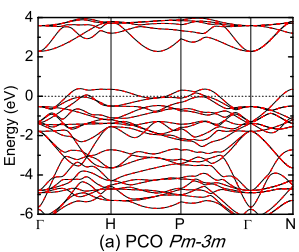
Fig. 6: (Color online) Band-structures of AFM PCO in  $Pm\bar{3}m$  and  $R3c$  phases as well as AFM PCO-CPO in  $R3$  phase computed in the LDA+ $U$  formalism with  $U=4$  eV. While the solid lines show the spin-up results, the dashed lines stand for spin-down. The Fermi energy level is set at zero as shown by the short-dashed lines.



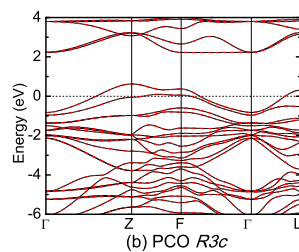




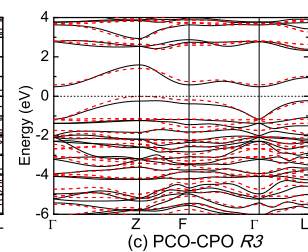




(a) PCO  $Pm-3m$



(b) PCO  $R3c$



(c) PCO-CPO  $R3$